How the alternating degeneracy in rotational Raman spectra of CO_2 and C_2H_2 reveals the vibrational temperature

D.C.M. van den Bekerom, J.M. Palomares Linares, E.M. van Veldhuizen, S. Nijdam, M.C.M. van de Sanden, and G.J. van Rooij

DIFFER, De Zaale 20, 5612AJ Eindhoven, The Netherlands

E-mail: g.j.vanrooij@differ.nl

https://doi.org/10.1364/AO.57.005694

Abstract. The contribution of higher vibrational levels to the rotational spectrum of linear polyatomic molecules with a center of symmetry (CO_2 & C_2H_2) is assessed. An apparent nuclear degeneracy is analytically formulated by vibrational averaging and compared to numerical averaging over vibrational levels. It enables inferring the vibrational temperature of the bending and asymmetric stretching modes from the ratio of even to odd peaks in the rotational Raman spectrum. The contribution from higher vibrational levels is already observable at room temperature as $\tilde{g}_{e/o} = 0.96/0.04$ for CO_2 and $\tilde{g}_{e/o} = 1.16/2.84$ for C_2H_2. The use of the apparent degeneracy to account for higher vibrational levels is demonstrated on spectra measured for a CO_2 microwave plasma in the temperature range of 300 to 3500K, and shown to be valid up to 1500K.

1. introduction

Rotational Raman Spectroscopy is employed to measure the rotational temperature and species densities in reactive gas mixtures such as combustion systems or plasmas. The technique is often used on diatomic gases such as N_2, H_2, and O_2[Drake and Rosenblatt, 1978] for measuring the temperature in the gas mixture. The spectrum of polyatomic molecules is typically too complex because of multiple rotational constants, resulting in complicated line structures in the rotational spectrum[Avila et al., 2003].

Our work concerns CO_2 plasma-conversion. Here CO_2 is the majority species, of which rotational and vibrational temperatures are to be diagnosed[Barrett and Weber, 1970, Brehmer et al., 2015, Klarenaar et al., 2015]. Fortunately CO_2, as well as C_2H_2, are linear polyatomic molecules that only have a single rotational constant and correspondingly a rotational spectrum similar to that of

diatomic molecules[Herzberg, 1950]. Nevertheless, high temperature or a vibration-rotation non-equilibrium requires the contribution of higher vibrational levels to be taken into account, which is the subject of this work.

The first rotational Raman spectra in a CO_2 plasma were recorded by Barrett and Weber[Barrett and Weber, 1970]. Although the CO_2-spectrum is commonly considered to contain only even-J rotational lines, they noted that odd-J peaks may appear due to the population of bending modes. With high enough spectral resolution, this becomes visible even at room temperature[Altmann and Strey, 1972]. At lower spectral resolution however, the population of odd-J levels could mistakenly be interpreted as broadening of the even-J peaks. Numerical models have been developed to account for the contribution of the vibrational levels to the rotational spectrum for both CO_2 [Schenk et al., 2005b, Schenk et al., 2005a, Vestin et al., 2008] and C_2H_2 [Bood et al., 2000]. However, at high (vibrational) temperature these models may have to include the spectra of hundreds of vibrational levels which greatly increases the computational power necessary for synthesis of the rotational Raman spectrum.

The explanation of the odd rotational lines appearing, lies in the symmetry of the vibrational levels. At low temperature, only the ground vibrational level is populated. In the ground state of CO_2, even rotational levels have s-symmetry and a degeneracy $g_s = 1$, while odd rotational levels have an a-symmetry and a degeneracy $g_a = 0$ For this reason, at low temperature the odd rotational lines are absent in the spectrum. Higher vibrational levels can have different symmetries resulting in even rotational levels that can have a and odd rotational levels that can have s symmetry. For these vibrational levels the degeneracy is also swapped correspondingly.

In this paper we show that the complexity of the CO_2 and C_2H_2 spectrum can be reduced to that of a diatomic rotational spectrum, in the sense that no explicit care has to be taken for individual higher vibrational levels. A direct relation between the ratio of even and odd-J rotational levels and the vibrational temperatures of the bending and asymmetric stretch modes is deduced. It allows to extract vibrational temperature information from rotational spectra simply from the ratio of even to odd J peaks. In rotation-vibrational equilibrium systems this represents a fast and easy temperature analysis. The methodology relies on an approximation of the average degeneracy, which in turn determines the density of rotational states. It is therefore applicable to both spontaneous rotational Raman scattering and rotational CARS.

2. Results

The analysis of the rotational spectrum will be performed in three different sections. In section 2.1 the experimental rotational spectrum in CO_2 is discussed. In section 2.2 the apparent nuclear degeneracy $\tilde{g}_{e/o}$, which determines the relative weights of even-J and odd-J components of the spectrum, is derived. Finally in section 2.3 some properties of $\tilde{g}_{e/o}$ will be discussed.

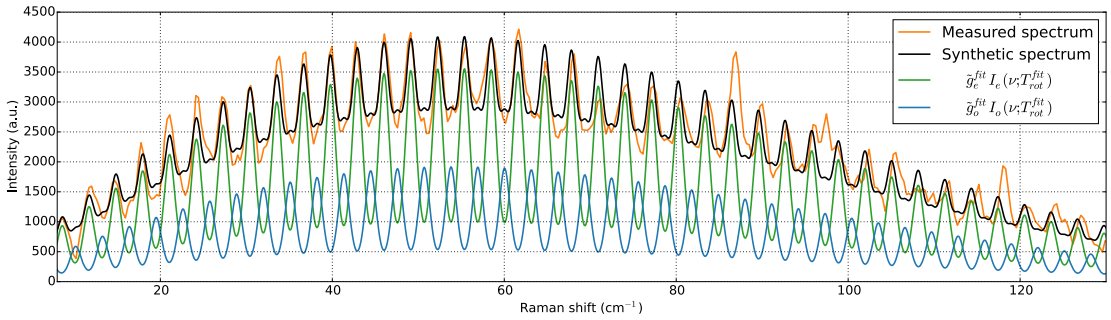

Figure 1. Typical measured rotational Raman spectrum of CO_2 at $T_{rot}^{fit} = 1375K$ (orange). The fitted synthetic spectrum (black) is the sum of an even and odd-J component (green and blue, respectively). The apparent nuclear degeneracy determines the fraction of the odd component of this spectrum. In this case the predicted fraction of the odd-J component was $\tilde{g}_o = 0.358$ while the fit determined the optimal value to be $\tilde{g}_o^{fit} = 0.350$. The anomalous peaks at 87, 98, and 119 cm^{-1} are due to noise from the intensifier.

2.1. High temperature rotational Raman spectrum in CO_2 plasma

Rotational Raman spectra were measured in CO_2 microwave plasma, which provided temperatures ranging from 300 K to 3500 K in a setup that was described previously[van Rooij et al., 2015, van den Bekerom et al., 2017]. Briefly, a 450 W microwave source produced microwaves at 2.45 GHz that were guided to an applicator, which was intersected by a quartz tube of 2 cm diameter containing the plasma. CO_2 was flowed at a rate of 2 slm at a pressure of 75 and 160 mbar. A 4W Nd:YAG laser produces 6 ns pulses at a 10 Hz repetition rate with a wavelength of 532 nm. This laser beam was focused at the center of the plasma. The scattered light was collected by a Triple Grating Spectrometer (TGS) to filter out the Rayleigh peak[van de Sande and van der Mullen, 2002, Carbone and Nijdam, 2015]. A pair of plano-convex lenses with a 95mm diameter and 600 mm focal distance were used to image the scattered light on a 250 μm slit. The light is then collimated to illuminate the first of three gratings with 1800 grooves per mm, resulting in a dispersion of 0.65 nm mm^{-1}. All lenses that were used were achromatic doublet lenses with the same diameter of 95 mm and focal distance of 600mm. After the first grating the light is imaged onto a 500 μm mask to block the Rayleigh line. The light is then collimated onto the second grating, which spectrally recombines the light, after which the light is focusing on an exit slit of 250 μm. Effectively, the first two gratings act as a notch filter for 532 nm. The blocking window, defined as blocking at least 98% of the Rayleigh light, has a width of 0.28 nm[van de Sande and van der Mullen, 2002]. The light is finally collimated onto a third grating, after which it is imaged onto a 16.5 mm wide iCCD camera, resulting in a 10 nm spectral window. This allows Raman shifts up to 130 cm^{-1} to be recorded in both the Stokes and Anti-Stokes branches. In a single acquisition an axial distance of about 11 mm can be recorded. To improve S/N, the raw spectra were axially binned

into 6 bins. The spectra were fitted separately for the 6 bins and separately for the Stokes and Anti-Stokes branches. The temperatures reported here are the average of the Stokes and Anti-Stokes fit, which typically did not differ more than 5%. The spectra of the highest temperatures were averaged for 20 minutes to achieve decent S/N. If a TGS is not available, a linear polarization filter may be used to attenuate the Rayleigh peak as well. Because the depolarization ratio of the Rayleigh line is small in CO_2, this will eliminate most of the Rayleigh signal, but at the cost of losing roughly half of the rotational Raman signal as well[Penney et al., 1974, Baas and van den Hout, 1979].

A rotational Raman spectrum measured at 150 W average power and a pressure of 75 mbar is shown in figure 1. The rotational temperature was determined to be 1375 K. By comparing spectra measured under similar conditions, it was found that spurious peaks appear randomly in the different spectra and thus cannot be due to spectral features. The anomalous peaks at 87, 98, and 119 cm^{-1} are therefore likely due to noise from the intensifier. From this spectrum it can be inferred that the rotational spectrum has a non-zero odd-J component because of higher vibrational levels being populated, as shall be motivated in section 2.2. Although the resolution was too low to completely resolve the odd rotational peaks, the presence of odd peaks is apparent as a reduced depth of the valleys between even peaks. The presence of odd-J rotational peaks is quantified by fitting the spectrum with an even-J and an odd-J components, where the weight of each component left as a fitting parameter:

$$I(\nu) = \tilde{g}_e^{fit} I_e(\nu; T_{rot}^{fit}) + \tilde{g}_o^{fit} I_o(\nu; T_{rot}^{fit}) \tag{1}$$

With T_{rot}^{fit} the fitted rotational temperature, I_e and I_o the even and odd component of the spectrum, respectively, and $\tilde{g}_e^{fit}$ and $\tilde{g}_o^{fit}$ the fitted apparent nuclear degeneracies of the even and odd-J levels respectively, with the constraint that $\tilde{g}_e^{fit} + \tilde{g}_o^{fit} = g_s + g_a = 1$ for CO_2. Throughout the paper, the tilde will be used for apparent values and the superscript *fit* for fitted parameters. Since $\tilde{g}_e^{fit} + \tilde{g}_o^{fit} = 1$ for CO_2, the apparent nuclear degeneracy can be directly used as the weighting factors for the even and odd components of the spectrum.

2.2. Derivation of apparent degeneracy

Let us consider the origin of the odd peaks in detail with the purpose to link the experimental values of $\tilde{g}_e^{fit}$ and $\tilde{g}_o^{fit}$ to vibrational excitation. The rotational energy $F_v(J)$ is generally a function of vibrational level and is given by:

$$F_v(J) = B_v J(J+1) + D_v J^2 (J+1)^2 \tag{2}$$

where B_v is the rotational constant of level v and D_v is the corresponding centrifugal distortion constant. Raman line positions are calculated from the term values $F_v(J)$ as $\nu(v, J) = F_v(J \pm 2) - F_v(J)$, and depend on the vibrational level via B_v and D_v. If the variation in B_v and D_v is small, the rotational spectrum can be approximated by using the values for the vibrational ground state B_0 and D_0, i.e. $F_v(J) = F_0(J)$.

For CO_2, the maximum change of B_v relative to the ground state rotational constant B_0 is smaller than 3% [Rothman and Young, 1981] for all vibrational levels below 10,000 cm^{-1}. For vibrational levels below 4,600 cm^{-1} this difference is only 1%. The rotational constant of CO_2 is thus assumed to be constant for different vibrational levels. Under this assumption the rotational peak positions are only a function of the rotational quantum J, regardless of their vibrational level. The observed line intensities at a Raman shift $\nu(J)$ can thus be written as the sum of the rotational spectra of all vibrational levels:

$$I(J) \propto \sum_v n_v g_{n,v}(J) S_{J,v} \exp -\frac{hcF_v(J)}{kT_{rot}} \tag{3}$$

Here n_v is the vibrational level density, $S_{J,v}$ is the scattering cross-section†, $g_{n,v}(J)$ is the nuclear spin degeneracy of the vibrational level v, and T_{rot} is the rotational temperature. The value of $g_{n,v}(J)$ alternates between even and odd rotational level for homonuclear diatomic molecules and linear molecules with a center of symmetry (CO_2, C_2H_2). Most importantly, this alternation may switch between vibrational levels in polyatomic molecules. The impact of this changing degeneracy in the summation of vibrational levels is illustrated in figure 2. Because the J-dependence of $g_{n,v}(J)$ is only determined by whether J is even or odd, we will replace it by $g_{e/o}$ in the following, where the subscript e is used for even-J and the subscript o is used for odd-J rotational levels, respectively.

Since the individual rotational lines of different vibrational levels overlap, eq 3 can be simplified by taking all terms that are only weakly dependent on the level v outside of the summation. We then follow the approach of Vestin et al.[Vestin et al., 2008] and assume that the polarizability anisotropy does not change for different vibrational levels, i.e. a constant cross section for all levels $S_{J,v} = S_J$. This reduces eq 3 to:

$$I(J) \propto n_0 \tilde{g}_{e/o} S_J \exp -\frac{hcF_0(J)}{kT_{rot}} \tag{4}$$

The subscript e and o are used for even and odd J rotational levels, respectively, and we have defined the apparent nuclear degeneracies:

$$\tilde{g}_{e/o} = \sum_v \frac{n_v}{n_0} g_{e/o,v} \tag{5}$$

We now move to the central argument of this paper, namely that this sum can be evaluated analytically by rewriting in terms of partition functions for each vibrational symmetry and applying the harmonic oscillator approximation. Details of this procedure are given in appendix Appendix A. We then arrive at the most important result of this paper, namely that the apparent nuclear degeneracies of CO_2 and C_2H_2 can be expressed in terms of their vibrational temperatures by:

$$CO_2 : \tilde{g}_{e/o} = \frac{1}{2} \pm \frac{1}{2} \left(\frac{1 - z_2}{1 + z_2}\right) \left(\frac{1 - z_3}{1 + z_3}\right) \tag{6}$$

† The factor $(2J + 1)$ is included in S_J here.

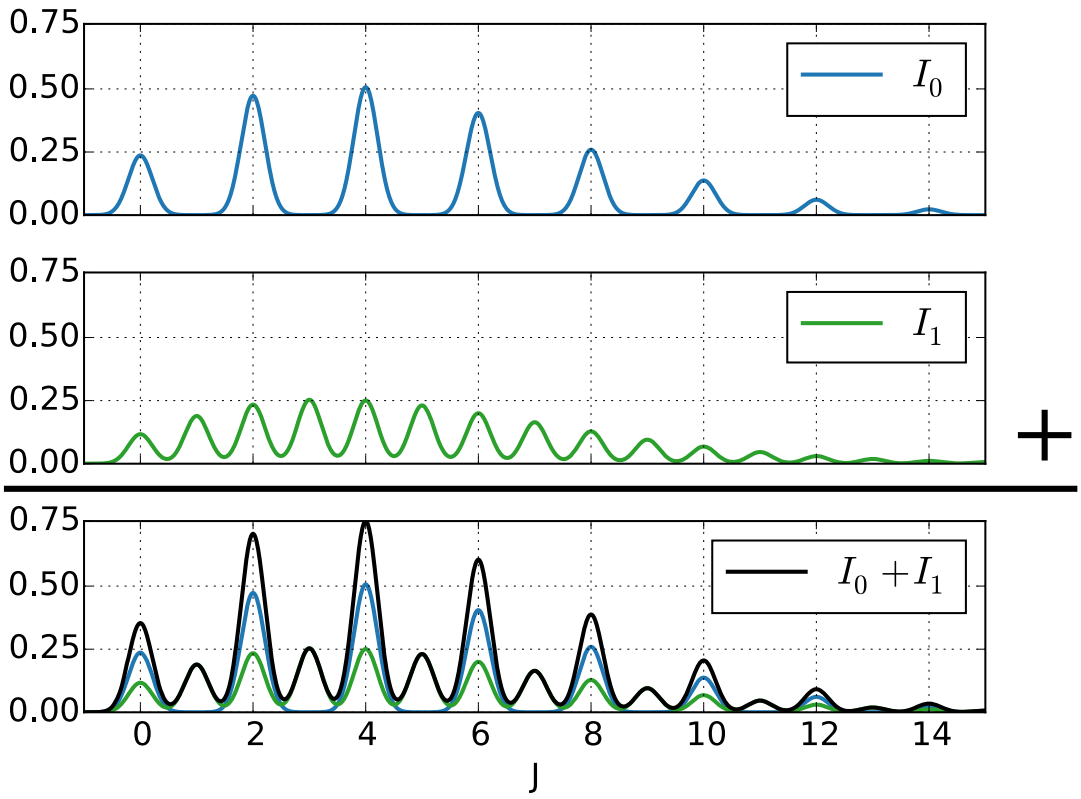

Figure 2. Synthetic spectra illustrating how the vibrational averaging produces odd lines. A rotational spectrum I_0 of a vibrational level with relative density $\frac{1}{2}$ and $g_{e/o} = 1/0$ (blue) is added to spectrum I_1 of another vibrational level with relative density $\frac{1}{4}$ and $g_{e/o} = 1/1$ (green). The sum spectrum $I_0 + I_1$ (black) then has a apparent nuclear degeneracy of $\tilde{g}_{e/o} = 0.75/0.25$. The blue and green lines in the bottom graph indicate the original I_0 and I_1 spectra.

$$C_2H_2 : \tilde{g}_{e/o} = 2 \mp \left(\frac{1-z_3}{1+z_3}\right)\left(\frac{1-z_4}{1+z_4}\right)\left(\frac{1-z_5}{1+z_5}\right) \tag{7}$$

The top sign is used for even and the bottom sign is used for odd J, respectively. The terms z_ν are the Boltzmann factors for normal mode ν with fundamental vibrational frequency ω_i referenced to the vibrational ground state (see table 1), and T_i the vibrational temperature of normal mode i, described by:

$$z_i = \exp -\frac{hc\omega_i}{kT_i} \tag{8}$$

The accuracy of eq 6 and 7 is assessed by comparing the calculated $\tilde{g}_{e/o}$ with the fit results $\tilde{g}^{fit}_{e/o}$ of fitted experimental spectra measured in our plasma reactor over a wide temperature range. The values of $\tilde{g}_o$ and $\tilde{g}^{fit}_o$ are compared as a function of T^{fit}_{rot} in figure 3. For temperatures below 1500K there is good agreement between measurement and analytical approximation. Above 1500K, measured apparent degeneracy $\tilde{g}^{fit}_o$ seems to be consistently higher than the approximated value.

Table 1. Fundamental vibrational frequencies for CO_2 and C_2H_2[Herzberg, 1950]. Symmetric stretch values are also tabulated for completeness. For the Fermi-resonant symmetric stretch in CO_2, the unperturbed energy is listed[Courtoy, 1957].

Normal mode	CO_2	C_2H_2
i	ω_i (cm^{-1})	ω_i (cm^{-1})
1	1341.5 (sym.)	3372.5 (sym.)
2	667.3 (bend.)	1973.5 (sym.)
3	2349.3 (asym.)	3294.85 (asym.)
4		611.70 (bend.)
5		729.15 (bend.)

An overestimation of $\tilde{g}_o^{fit}$ would indicate a vibrational non-equilibrium, but at this high temperature the uncertainty is too high to be conclusive. The uncertainty in this high temperature regime is increased because of peaks overlapping due to increased temperature broadening, and reduced signal intensity due to low number density. To illustrate the temperature dependence of the signal strength, rotational spectra measured at 430K, 1380K and 2670K are plotted in figure 4. In this figure it is clearly visible that at 2670K the random fluctuations are larger than the alternating peak height of even and odd rotational peaks. While the spectra shown were taken at the highest resolution possible in the current setup, increasing the spectral resolution would facilitate the separation of even and odd peaks, making this procedure more reliable. At high rotational numbers however, peaks will always have some overlap because of the spread in rotational constants, discussed in section 3. Note that at higher resolution, the loss in signal intensity will have to be offset by e.g. using a higher laser power or increased averaging. Another possible way to increase the signal intensity may be to use a coherent scheme like rotational CARS [Bood et al., 2000, Schenk et al., 2005b, Schenk et al., 2005a]. Instead of leaving $\tilde{g}_o^{fit}$ as a free fitting parameter, in cases where thermal equilibrium is to be expected it is better to replace $\tilde{g}_{e/o}^{fit}$ with $\tilde{g}_{e/o}$ in eq 1 to reduce the uncertainty in the fitted rotational temperature T_{rot}^{fit}.

2.3. Properties of apparent degeneracy

Having established an explicit description for the apparent nuclear degeneracies, we investigate the newly found relationship between $\tilde{g}_{e/o}$ and the vibrational temperature of eq 8.

The first property to notice is that the apparent degeneracy is not affected by the symmetric stretch temperature. Although this result is not directly clear by summation of the spectra using eq 3, it is a direct result of the fact that all symmetric stretch levels can only have the σ_g^+ symmetry. Since the nuclear degeneracy of a vibrational level depends on the molecular symmetry, which does not change for any particular ν_1 level,

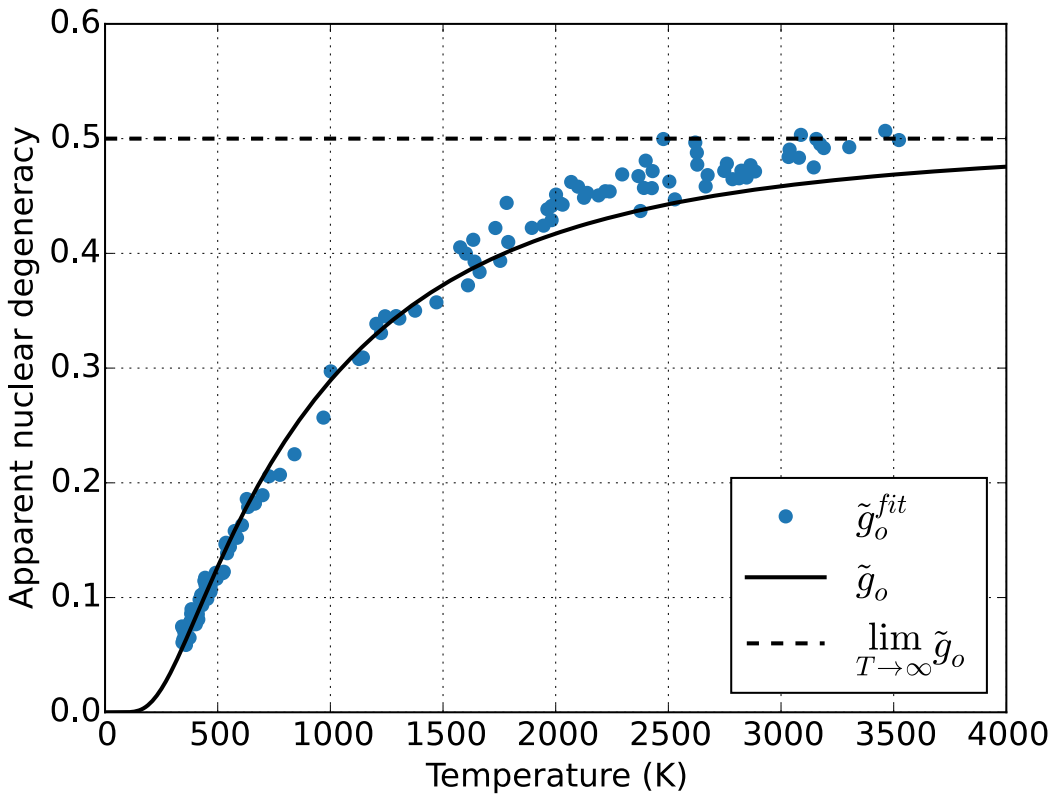

Figure 3. Comparison of the fraction of odd-J levels predicted by eq. 6 (black solid line), and determined by the fit $\tilde{g}_o^{fit}$ (blue dots), respectively, as a function of rotational temperature. The highest possible fraction for Boltzmann distributed vibrational levels in CO_2 is $\frac{1}{2}$.

the distribution of the symmetric stretch levels will not influence $\tilde{g}_{e/o}$. This is also the reason why diatomic molecules do not have a varying degeneracy for higher vibrational levels.

Next, we will reason that the cross-section is not altered by the varying degeneracies at higher levels, so that the total signal level is still a good measure for the species density. By adding the even and odd parts of eq. 6 or 7, we find that in general $\tilde{g}_e + \tilde{g}_o = g_s + g_a$. For CO_2, $g_s = 1$ and $g_a = 0$. Since both g_s and g_a are constants that have no temperature dependence, including the alternating degeneracy for higher vibrational levels will not influence the average cross-section. There remains a small dependency of the cross-section on the vibrational level via the ℓ-dependent Placzek-Teller coefficients[Long, 2002], which reduces the cross-section for high ℓ and low J. However, this is a minor effect amounting to a 3% overestimation of the average cross-section at $2000K$. Therefore, the total band intensity is a direct measure for the total number density, even when hot-bands are included.

The ratio of even to odd rotational levels can be an indicator for non-Boltzmann

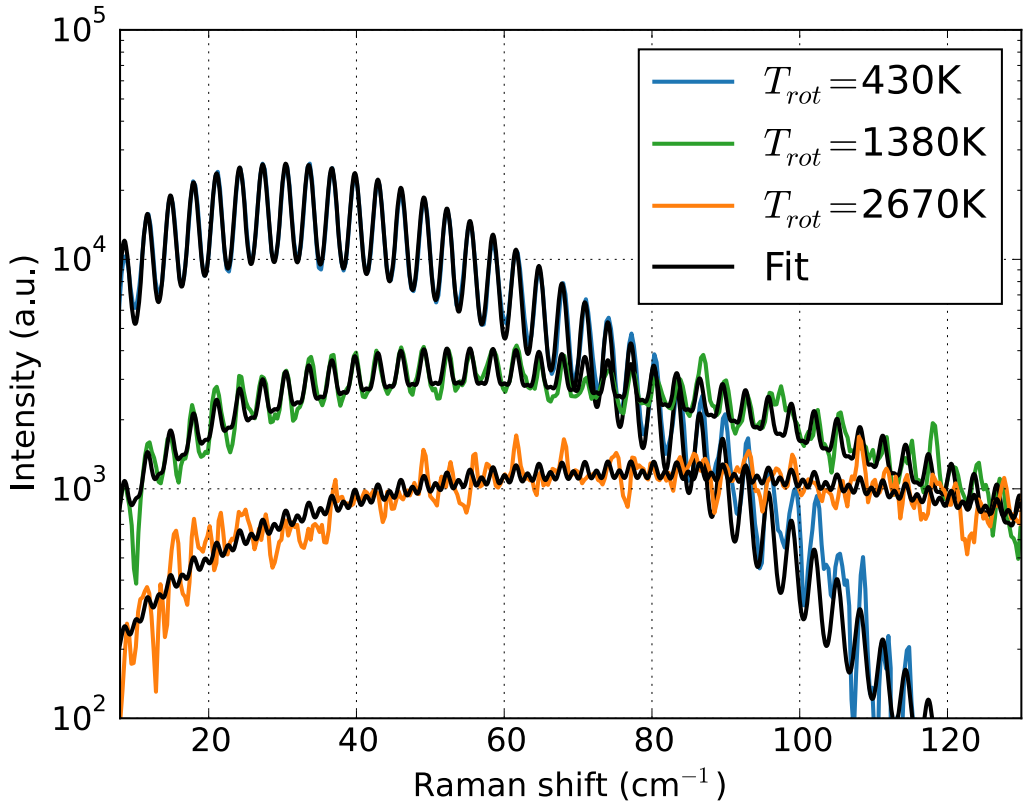

Figure 4. Fit of the rotational Raman spectrum at three different temperatures: 430K, 1380K, and 2670K. At higher temperatures, S/N is greatly reduced, resulting in overestimation of the odd-J component. The anomalous peaks are due to noise from the intensifier.

distributed vibrational levels. In the limit for high temperatures, eq 6 and 7 yield $\tilde{g}_e = \tilde{g}_o$, which for CO_2 is equal to $\frac{1}{2}$. The implication is that for a system where the vibrational levels are Boltzmann distributed, the level e or o that has the highest degeneracy at low temperatures will always remain the highest, no matter how high the (vibrational) temperature. This condition can only be violated if the vibrational levels do not follow a Boltzmann distribution. Because bending mode levels will always have $g_e = g_o$ (see appendix Appendix A), this method is exclusively sensitive to the overpopulation of asymmetric stretch levels. However, the distribution needs to deviate far from a Boltzmann distribution for this to happen so it is well possible to have a non-Boltzmann distribution while not violating this condition. Finally, already at room temperature contributions of higher vibrational levels can be significant. Taking into account higher vibrational levels, the apparent even/odd degeneracy is not equal to the symmetric/asymmetric degeneracy ($\tilde{g}_{e/o} \neq g_{s/a}$). We therefore assess the values of the apparent degeneracy at room temperature. This is important because bending modes typically have a low energy and can be significantly populated already at

low temperatures. At $300K$ we find $\tilde{g}_{e/o} = 0.96/0.04$ instead of $1/0$ for CO_2, and $\tilde{g}_{e/o} = 1.16/2.84$ instead of $1/3$ for C_2H_2. Although the correction is small, it may not be negligible. We therefore recommend that the apparent nuclear degeneracy is *always* used in favor of the ground state values, even at lower temperatures.

3. Implementing the vibrational dependence of rotational constants

In the derivation of eq 4 it was assumed that the rotational constant is independent of the vibrational level. In this section, we will assess how accurate this assumption is. Assuming a constant B_v overlooks two important features in the approximated spectrum: 1. A shift in the peak positions because of a changing average rotational constant with increasing temperature, and 2. An apparent broadening of the rotational peaks as a result of not having a single rotational constant, but rather a distribution of rotational constants that results in a 'smearing' of the rotational peaks. Both effects become more pronounced at higher J.

The shift in peak positions can be corrected by using an apparent or average rotational constant $\tilde{B}$ instead of the ground state value B_0, which can be a function of temperature. The apparent broadening is modelled as a Gaussian function that is added to other pre-existing broadening mechanisms, with a standard deviation $\tilde{\sigma}_J$ that increases with the rotational quantum number J:

$$\tilde{\sigma}_J = J\tilde{\sigma}_1 \tag{9}$$

with $\tilde{\sigma}_J$ the apparent broadening, J the rotational quantum number and $\tilde{\sigma}_1$ the initial apparent broadening for $J = 1$.

To determine the values for $\tilde{B}$ and $\tilde{\sigma}_1$, first reference synthetic spectra were generated in a range of temperatures from 300K to 2000K with 100K increments. These fully detailed synthetic spectra include all features as described by Vestin[Vestin et al., 2008]. Spectroscopic constants were taken from Courtoy[Courtoy, 1957], but can also be found in the paper by Chedin[Chedin, 1979]. At each temperature, the reference spectrum was fitted by an approximated spectrum as described by eq 1, but amended with an apparent broadening described in eq 9. The temperature was used as an input parameter and was not fitted in this case, while the apparent rotational constant $\tilde{B}$ and the initial apparent broadening $\tilde{\sigma}_1$ were used as fitting parameters, as was the apparent nuclear degeneracy like in eq 1. Separate fitting parameters were used for the even and odd-J components of the spectrum to further improve the accuracy of the model. At each temperature approximate model is fitted to the fully detailed reference spectrum, resulting in the following fitting parameters: $\tilde{g}_o^{fit} = 1 - \tilde{g}_e^{fit}$, $\tilde{B}_e^{fit}$, $\tilde{B}_o^{fit}$, $\tilde{\sigma}_{1,e}^{fit}$, and $\tilde{\sigma}_{1,o}^{fit}$. These optimized values are presented in figure 5. Apart from determining the optimal values for apparent rotational constant and broadening, this allows us to verify the accuracy of eq. 6 without any of the experimental uncertainties that were present in the data shown in figure 3. The analytical expression for the apparent degeneracy predicts the optimal value with high accuracy. The apparent

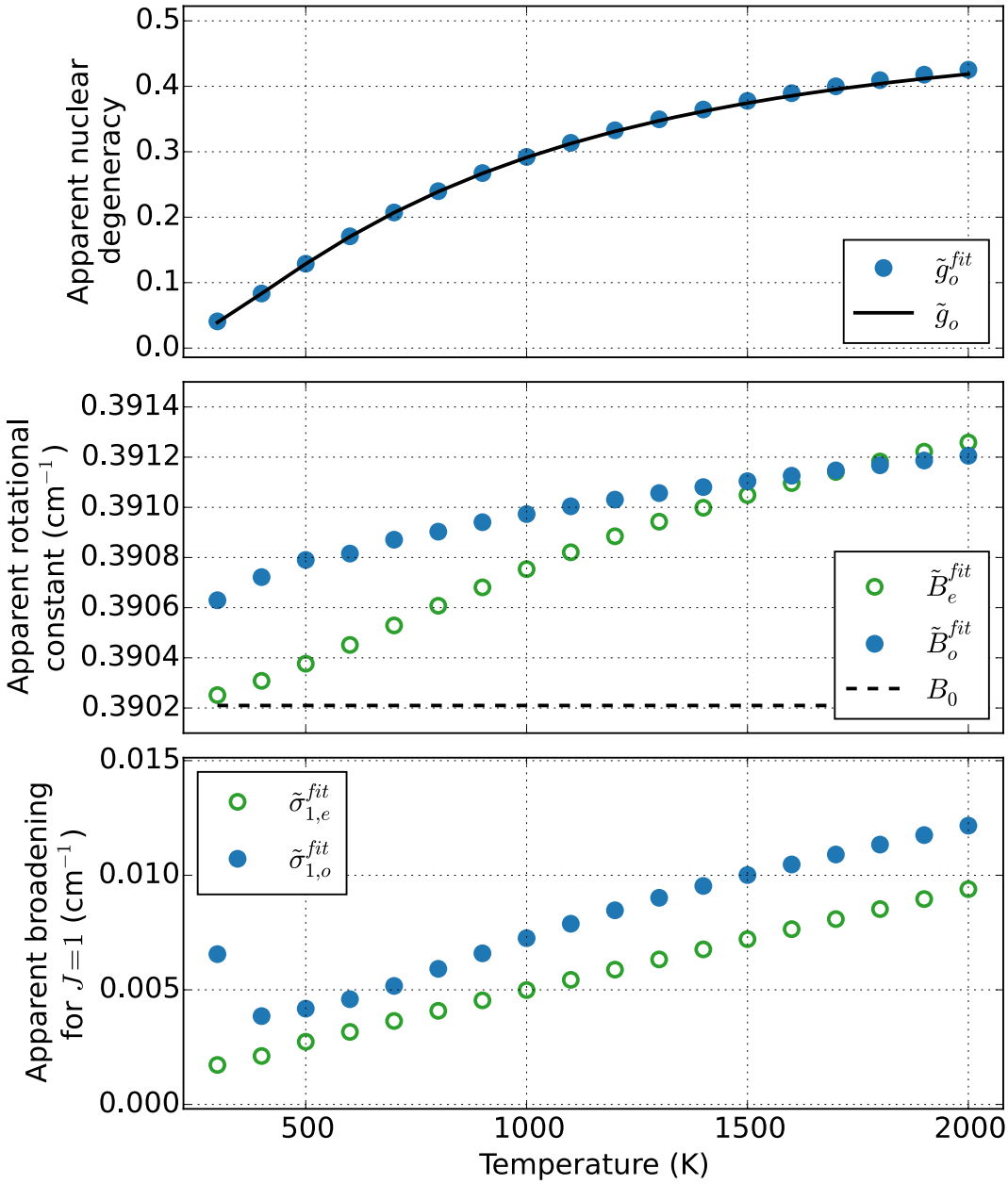

Figure 5. Comparison of the optimally fitted parameters in the approximated model as a function of temperature. Top: the fitted apparent degeneracy (blue dots) compared to the analytical expression (solid black line). Middle: apparent rotational constants for even (green) and odd (blue) components, respectively. Bottom: apparent broadening for even (green) and odd (blue) components, respectively.

rotational constants show an appreciable deviation from B_0 at high temperatures, so that the use of apparent rotational constants is warranted. To find how well the approximated model reproduces the real spectrum, we will now compare three models: i) a 'naive'

model with $\tilde{g}_e = 1$ and $\tilde{g}_o = 0$, ii) a model with an apparent degeneracy described by eq 6, and iii) the improved model including additionally apparent rotational constants and broadening, using the values displayed in figure 5. These three models were fitted to the fully detailed spectra with a Gaussian lineshape of 1 cm^{-1} FWHM. Each model was fitted to the synthetic spectra for a range of temperatures from 300 to 2000 K with only the temperature as fitting parameter. In figure 6 the results of these fits are shown. In the top plot, the error of the fitted temperature relative to the actual temperature is plotted. Model 1 produces large temperature errors even at low temperatures. This emphasizes the need for including the contribution of higher vibrational levels by using the apparent degeneracy even at moderate to low temperatures, as discussed at the end of section 2.3. For example, at 550K the temperature error is already over 10% if only the vibrational ground state values for g_e and g_o are used. Model 2 and model 3 perform about equally well, with a temperature error below 3% for temperatures below 1500 K. In the bottom graph the mismatch between the synthetic and fitted spectrum is plotted. This is defined here as the fraction of area of the fit and synthetic spectrum that are not overlapping. The mismatch is significantly smaller for model 3. In conclusion, model 2 and model 3 will result in a similarly accurate fitted temperature, but in model 3 the residue will be lower.

4. Conclusions

We have demonstrated that it is possible to greatly simplify the calculation of the rotational spectrum of centrosymmetric, linear polyatomic molecules, by separating the rotational spectrum in an even and odd component with different weights. This approximated spectrum was able to reproduce experimental spectra to a satisfactory degree. The weights can be calculated by vibrationally averaging the nuclear spin degeneracy over all vibrational levels. The resulting apparent degeneracy $\tilde{g}_{e/o}$ can be evaluated analytically and provides a direct link to the temperature of the bending and asymmetric stretch vibrational modes. This either eliminates the weight of the even/odd component as a fitting parameter in the simplified model, or it provides the option to use the ratio of even and odd rotational peaks as an indicator vibrational non-equilibrium. The temperature error introduced by not including higher vibrational levels quickly increases with temperature, so it is recommended that the apparent degeneracy is used in favor of the ground vibrational state degeneracy even at low temperatures.

5. References

[Altmann and Strey, 1972] Altmann, K. and Strey, G. (1972). Ein verfahren zur computer-simulation der rotationsstruktur von raman banden. *Z. Naturforsch.*, 27a:65–67.

[Avila et al., 2003] Avila, G., Tejeda, G., Frnndez, J. M., and Montero, D. (2003). The rotational Raman spectra and cross sections of H_2O, D_2O, and HDO. *J. Mol. Spectrosc.*, 220.

[Baas and van den Hout, 1979] Baas, F. and van den Hout, K. D. (1979). Measurements of depolarization rations and polarizability anisotropies of gaseous molecules. *Physica A*, 95A.

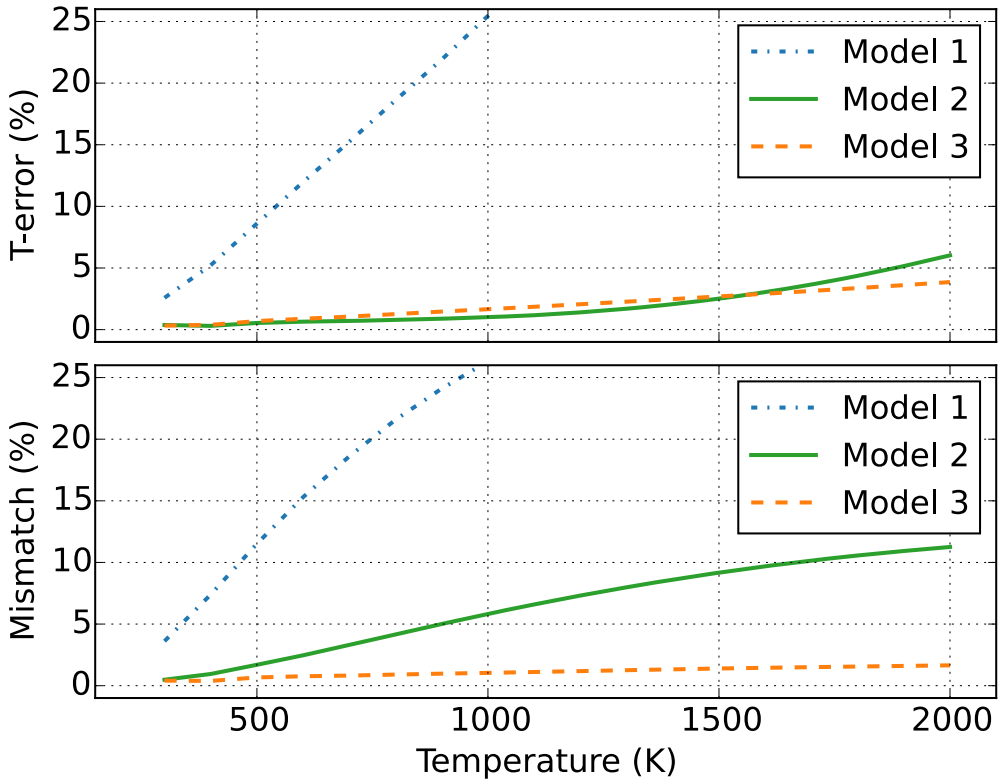

Figure 6. The relative error in the fitted temperature (top) and the mismatch of the fitted function with the full detail synthetic spectrum (bottom) for temperatures from 300 to 2000K for three models. Model 1: $\tilde{g}_{e/o} = 1/0$, Model 2: $\tilde{g}_{e/o}$ is described by eq 6. Model 3: Optimized apparent degeneracy, rotational constant and broadening as displayed in 5.

[Barrett and Weber, 1970] Barrett, J. J. and Weber, A. (1970). Pure-rotational Raman scattering in a CO_2 electric discharge. *J. Opt. Soc. Am.*, 60(1).

[Bood et al., 2000] Bood, J., Bengtsson, P.-E., and Aldn, M. (2000). Temperature and concentration measurements in acetylene-nitrogen mixtures in the range 300-600K using dual-broadband rotational CARS. *Appl. Phys. B*, 70:607–620.

[Brehmer et al., 2015] Brehmer, F., Welzel, S., Klarenaar, B. L. M., van der Meiden, H. J., van de Sanden, M. C. M., and Engeln, R. (2015). Gas temperature measurement in transient CO_2 plasma measured by raman scattering. *J. Phys. D*, 48.

[Carbone and Nijdam, 2015] Carbone, E. and Nijdam, S. (2015). Thomson scattering on non-equilibrium low density plasmas: principles, practice and challenges. *Plasma Phys. Control. Fusion*, 57.

[Chedin, 1979] Chedin, A. (1979). The carbon dioxide molecule: Potential, spectroscopic, and molecular constants from its infrared spectrum. *J. Mol. Spectrosc.*, 76.

[Courtoy, 1957] Courtoy, C.-P. (1957). XII. The spectrum of $C^{12}O_2^{16}$ between 3500 and 8000 cm^{-1} and molecular constants. *Can. J. Phys.*, 35.

[Drake and Rosenblatt, 1978] Drake, M. C. and Rosenblatt, G. M. (1978). Rotational raman scattering from premixed and diffusion flames. *Combustion and flame*, 33:179–196.

[Harris and Bertolucci, 1978] Harris, D. C. and Bertolucci, M. D. (1978). *Symmetry and Spectroscopy:*

An Introduction to Vibrational and Electronic Spectroscopy. Dover Publications, Inc., New York.

[Herzberg, 1950] Herzberg, G. (1950). *Molecular spectra and molecular structure Volume II: Infrared and Raman Spectra of Polyatomic Molecules*. Krieger Publishing Company, Malabar, Florida.

[Klarenaar et al., 2015] Klarenaar, B. L. M., Brehmer, F. K., Welzel, S., van der Meiden, H. J., van de Sanden, M. C. M., and Engeln, R. A. H. (2015). Note: Rotational raman scattering on CO_2 using a volume bragg grating as a notch filter. *Rev. Sci. Instruments*, 86.

[Long, 2002] Long, D. (2002). *The Raman Effect: A Unified Treatment of the Theory of Raman Scattering by Molecules*. John Wiley & Sons Ltd.

[Penney et al., 1974] Penney, C. M., Peters, R. L. S., and Lapp, M. (1974). Absolute rotational Raman cross-sections for N_2, O_2, and CO_2. *J. Opt. Soc. Am.*, 64.

[Rothman and Young, 1981] Rothman, L. S. and Young, L. D. G. (1981). Infrared energy levels and intensities of carbon dioxide – II. *J. Quant. Spectrosc. Radiat. Transfer*, 25.

[Schenk et al., 2005a] Schenk, M., Seeger, T., and Leipertz, A. (2005a). Simultaneous and time-resolved temperature and relative CO_2-N_2 and O_2-CO_2-N_2 concentration measurements with pure rotational coherent anti-stokes Raman scattering for pressures as great as 5 MPa. *Appl. Optics*, 44(26).

[Schenk et al., 2005b] Schenk, M., Seeger, T., and Leipertz, A. (2005b). Time-resolved CO_2 thermometry for pressures as great as 5 MPa by use of pure rotational coherent anti-stokes Raman scattering. *Appl. Optics*, 44(31).

[van de Sande and van der Mullen, 2002] van de Sande, M. J. and van der Mullen, J. J. A. M. (2002). Thomson scattering on a low-pressure, inductively-coupled gas discharge lamp. *J. Phys. D: Appl. Phys.*, 35.

[van den Bekerom et al., 2017] van den Bekerom, D. C. M., den Harder, N., Minea, T., Gatti, N., Linares, J. P., Bongers, W. A., van de Sanden, M. C. M., and van Rooij, G. J. (2017). Non-equilibrium microwave plasma for efficient high-temperature chemistry. *J. Vis. Exp.*, 126.

[van Rooij et al., 2015] van Rooij, G. J., van den Bekerom, D. C. M., den Harder, N., Minea, T., Berden, G., Bongers, W. A., Engeln, R., Graswinckel, M. F., Zoethout, E., and van de Sanden, M. C. M. (2015). Taming microwave plasma to beat thermodynamics in co$_2$ dissociation. *Faraday Discuss.*, 183.

[Vestin et al., 2008] Vestin, F., Nilsson, K., and Bengtsson, P.-E. (2008). Validation of a rotational coherent anti-stokes Raman spectroscopy model for carbon dioxide using high-rsolution detection in the temperature range 294-1143K. *Appl. Optics*, 47(11).

Appendix A. Derivation of apparent degeneracy

In this section we elaborate on the derivation of eq 5 to eq 7. We start by investigating the vibrationally dependent nuclear degeneracy $g_{e/o,v}$ in more detail, followed by the evaluation of the sum over the vibrational levels. This results in a general expression for $\tilde{g}_{e/o}$ that is applicable to any molecule that is in the $D_{\infty h}$ point group, i.e. linear and centrosymmetric.

Appendix A.1. Vibrational symmetry

First we will identify the symmetries of the vibrational normal modes. For non-degenerate vibrations, i.e. the symmetric and asymmetric stretch, even wave functions are totally symmetric and odd wave functions have the symmetry of the vibration[Harris and Bertolucci, 1978]. This means that the symmetric stretch has always symmetry $\Gamma_{\nu_s} = \sigma_g^+$ regardless of its level. It also explains why the degeneracy

Table A1. Symmetry of vibrational normal modes

Normal mode	σ_g^+	σ_u^+	π
ν_s (sym.)	*always*		
ν_{as} (asym.)	*v even*	*v odd*	
δ_d (bend.)	$\ell = 0$		$\ell \neq 0$

Table A2. Direct product for symmetries of vibrational normal modes

$\otimes$	σ_g^+	σ_u^+	π
σ_g^+	Σ_g^+	Σ_u^+	Π
σ_u^+	Σ_u^+	Σ_g^+	Π
π	Π	Π	Π

for a diatomic molecule does not change with temperature: All its possible vibrational modes (i.e. the single symmetric stretch) have the same symmetry σ_g^+, so increasing the temperature does not change the symmetry fractions. The asymmetric stretch alternates between $\Gamma_{\nu_{as}} = \sigma_g^+$ for even and $\Gamma_{\nu_{as}} = \sigma_u^+$ for odd vibrational levels.

For the degenerate vibration, i.e. the bending mode, the symmetry depends on the angular momentum quantum number ℓ and is $\Gamma_{\delta_d} = \sigma_g^+, \pi_u, \delta_g, \phi_u, ...$ for $\ell = 0, 1, 2, 3, ...$, respectively [Harris and Bertolucci, 1978]. Except for σ_g^+, all these representations are doubly degenerate in that for each J they represent two rotational levels. With respect to rotational levels, the only thing that distinguishes the π_u, δ_g, ϕ_u,... symmetries is that rotational levels with $J < |\ell|$ are absent. By ignoring this difference, we can consider all these symmetries as the same and bunch them together in the π_u-symmetry. In addition, as shall be motivated in section Appendix A.2, in terms of rotational levels there is no distinction between π_g or π_u, so that the g/u-label will be dropped for the π-symmetry. The bending mode symmetry then becomes $\Gamma_{\delta_d} = \sigma_g^+$ for $\ell = 0$ and $\Gamma_{\delta_d} = \pi$ for $\ell \neq 0$. In section Appendix A.3.2 we will assess the error that is introduced by grouping together all degenerate symmetries into a single π-symmetry. The symmetries of the vibrational normal modes are summarized in table A1.

The molecular symmetry is determined by the direct product of the symmetries of the individual vibrational normal modes:

$$\Gamma_v = \prod_i^{\otimes} \Gamma_i \tag{A.1}$$

Here Γ_i is the symmetry of some normal mode i. In table A2 the direct products of relevant vibrational symmetries are tabulated. We follow the convention of using small Greek letters for normal mode symmetries, and capital letters for the molecular symmetry.

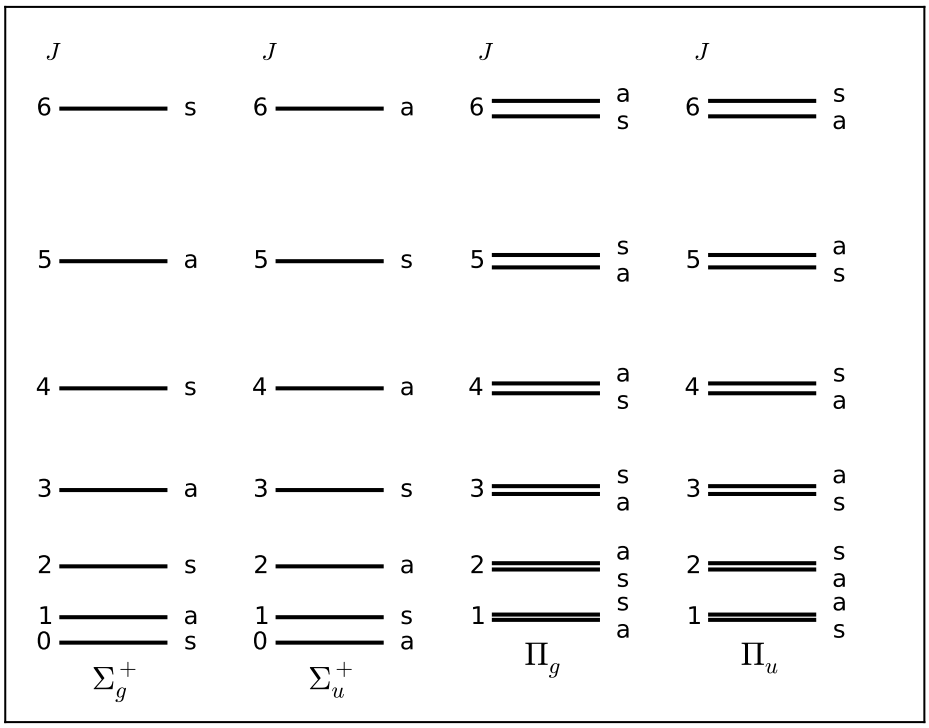

Figure A1. The symmetry of rotational levels for different symmetry representations of the vibrational mode[Herzberg, 1950].

Appendix A.2. Rotational symmetry and nuclear degeneracy

We return to evaluating the following sum:

$$\tilde{g}_{e/o} = \sum_v \frac{n_v}{n_0} g_{e/o,v} \tag{A.2}$$

The value of $g_{e/o,v}$ depends on the symmetry of the rotational level (s/a), which in turn depends on the symmetry of the vibrational level[Herzberg, 1950], as is shown in figure A1. Because bending vibrations are doubly degenerate, there are two rotational levels for each J in the Π-symmetry; one with s and one with a rotational symmetry. Since this is the case for both the Π_g- and Π_u-symmetry, we will ignore the g/u label in a Π-symmetry. We thus find that there are three different expressions possible for $g_{e/o,v}$ depending on the vibrational symmetry Γ_v of the molecule:

$$g_{e/o,v} = \begin{cases} g_{s/a}, & \Gamma_v = \Sigma_g^+ \\ g_{a/s}, & \Gamma_v = \Sigma_u^+ \\ \frac{1}{2}(g_s + g_a), & \Gamma_v = \Pi \end{cases} \tag{A.3}$$

The double degeneracy in the Π-symmetry is due to the fact that the ℓ-quantum number can be positive or negative. Since we will later explicitly distinguish between

positive and negative ℓ, the Π-symmetry degeneracies are halved. Eq A.2 can now be evaluated by taking the sums for the Σ_g^+, Σ_u^+, and Π vibrational symmetries, respectively:

$$\tilde{g}_{e/o} = g_{s/a}\frac{Q_{\Sigma_g^+}}{Q_{vib}} + g_{a/s}\frac{Q_{\Sigma_u^+}}{Q_{vib}} + \frac{1}{2}(g_s + g_a)\frac{Q_\Pi}{Q_{vib}} \tag{A.4}$$

Here Q_{Γ_v} is the partition function that counts all molecules with some vibrational symmetry $\Gamma_v = \Sigma_g^+, \Sigma_u^+$, or Π, and Q_{vib} is the vibrational partition function. Since the molecules can only have one of the three symmetries Σ_g^+, Σ_u^+, and Π, their partition functions count every possible vibrational state, i.e.:

$$Q_{vib} = Q_{\Sigma_g^+} + Q_{\Sigma_u^+} + Q_\Pi \tag{A.5}$$

This is used to eliminate Q_Π from eq A.4:

$$\tilde{g}_{e/o} = \frac{1}{2}(g_s + g_a) \pm \frac{1}{2}(g_s - g_a)\frac{\Delta Q_{\Sigma^+}}{Q_{vib}} \tag{A.6}$$

The plus sign is used for even J and the minus sign is used for odd J, and we have defined $\Delta Q_{\Sigma^+} = Q_{\Sigma_g^+} - Q_{\Sigma_u^+}$. All that remains is thus finding an expression for ΔQ_{Σ^+}.

Since the symmetry of the molecule depends on that of its normal modes, calculating the symmetry partition functions $Q_{\Sigma_g^+}$ and $Q_{\Sigma_u^+}$ is only possible if we have more information on the normal mode symmetry partition functions first. In the next section we will therefore derive the relevant symmetry partition functions for the three different normal modes in a linear molecule: symmetric stretch (ν_s), asymmetric stretch (ν_{as}) and bending mode (δ_d).

Appendix A.3. Vibrational symmetry partition functions

First, the calculation of the 'standard' vibrational partition functions is revisited. The calculation is then extended to the vibrational partition functions with a given symmetry. The partition function for a vibrational normal mode i is calculated in general by summing the Boltzmann factors for the vibrations:

$$Q_i = \sum_{v=0}^{N} g(v) \exp -\frac{hcG_0(v)}{kT_i} \tag{A.7}$$

here $g(v)$ is the degeneracy of the vibrational level (not to be confused with the rotational degeneracy) and $G_0(v)$ the vibrational energy of the level v with respect to the ground vibrational level. In the harmonic oscillator approximation, all higher order v terms except for the linear are ignored in $G_0(v)$. As a result, the energy spacing $G_0(v+1) - G_0(v)$ is constant for any v. Therefore the sum can be evaluated as a geometric series. We shall first calculate the partition functions for the non-degenerate vibrations, and then focus on the more complicated degenerate partition functions.

Appendix A.3.1. Non-degenerate vibrations For non-degenerate vibrations $g(v) = 1$ for every level v, so by using the harmonic oscillator approximation, eq. A.7 can be evaluated as:

$$Q_i = \sum_{v=0}^{\infty} {z_i}^v = \frac{1}{1 - z_i}, \quad i \in \nu_s, \nu_{as} \tag{A.8}$$

with $z_i = \exp -\frac{hc\omega_i}{kT_i}$ the Boltzmann factor, ω_i the energy of the fundamental vibration ($v_i = 1$) with respect to the ground vibrational level in cm^{-1} and T_i the vibrational temperature of normal mode i. The notation $i \in \nu_s, \nu_{as}$ is used to state that this result is valid for the symmetric (ν_s) and asymmetric (ν_{as}) stretch. As mentioned earlier, a symmetric stretch normal mode can only have the σ_g^+ symmetry. Consequently, for the symmetric stretch the σ_g^+ symmetry partition function is equal to the normal mode partition function:

$$Q_{i,\sigma_g^+} = Q_i, \quad i \in \nu_s \tag{A.9}$$

According to table A1 the asymmetric stretch can have one of two symmetries: σ_g^+ or σ_u^+. Since all levels with an even quantum have a σ_g^+ symmetry we can write for its symmetry partition function:

$$Q_{i,\sigma_g^+} = \sum_{k=0}^{\infty} {z_i}^{2k} = \frac{1}{1 + z_i} Q_i, \quad i \in \nu_{as} \tag{A.10}$$

Here we have expressed the result in terms of the normal mode partition function. As there are only two possible symmetries for the asymmetric stretch, the molecules that have σ_u^+ symmetry are all the molecules in the ν_{as} normal mode that are *not* counted by Q_{i,σ_g^+}:

$$Q_{i,\sigma_u^+} = Q_i - Q_{i,\sigma_g^+} = \frac{z_i}{1 + z_i} Q_i, \quad i \in \nu_{as} \tag{A.11}$$

Appendix A.3.2. Degenerate vibrations The partition functions for degenerate vibrations (bending modes) are less straightforward to calculate because of the double degeneracy. To visualize how the levels of the bending mode are distributed, it is insightful to consider the bending mode as two separate orthogonal modes H and V. When adding quanta to the δ_d mode, they can be added independently to the H or the V mode. By tabulating the resulting states, we establish the blue table in figure A2. In this table, states in the NE-SW diagonals have the same number of quanta and therefore correspond to the states with the same vibrational quantum v. The NW-SE diagonals correspond to states with the same ℓ quantum number that have the same symmetry. It should be emphasized that this table cannot be taken too literally since the horizontal and vertical bending modes cannot be distinguished like this, but it helps to account for the different levels in the bending mode. By counting the amount of states in the NE-SW diagonals we find the well known result that the vibrational degeneracy in level

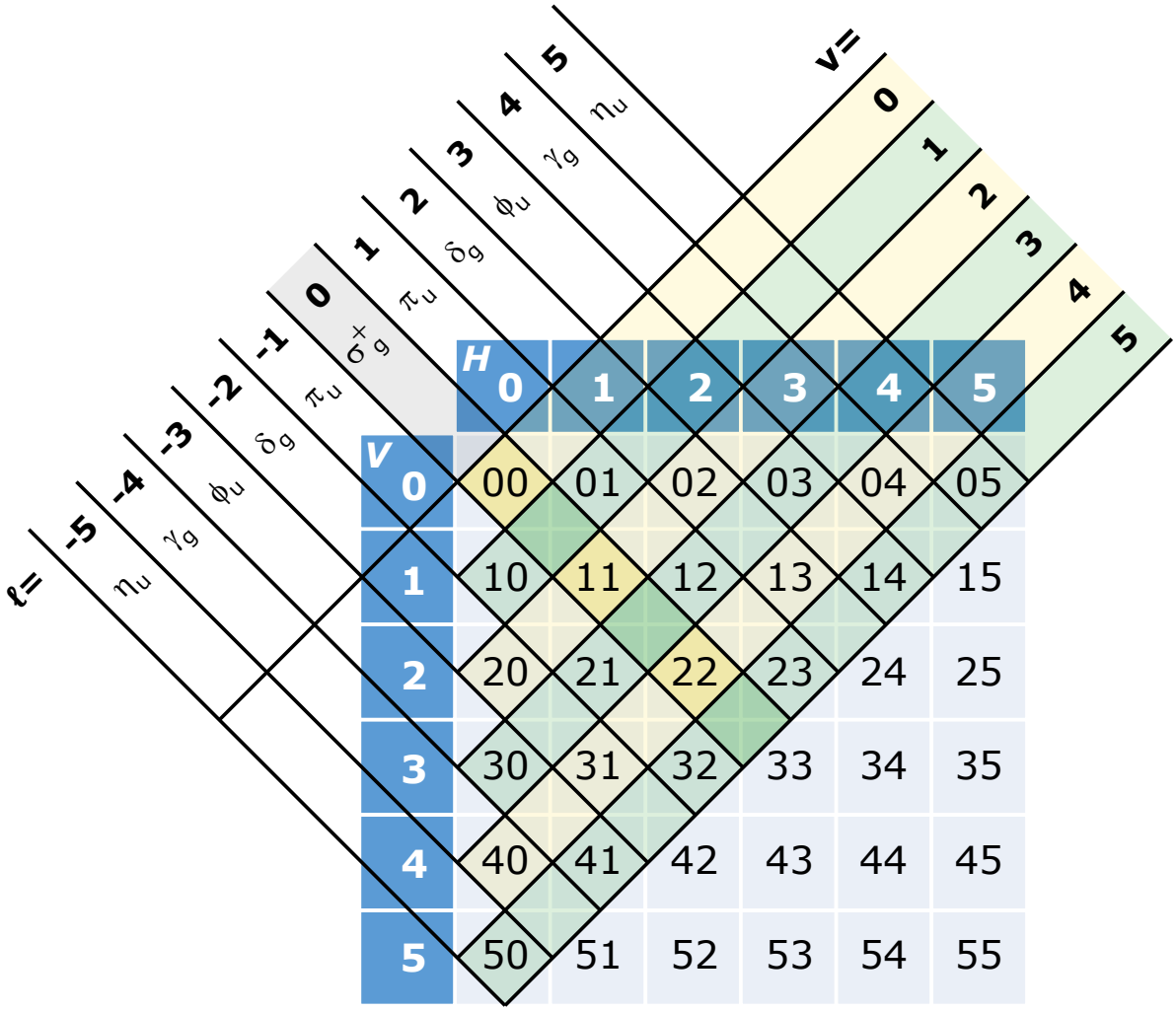

Figure A2. By considering the bending mode as two non-degenerate modes H and V all possible levels can be tabulated. We can then recognize that each level in the same NE-SW diagonal has the same number of quanta v. The states in the same NW-SE diagonal have the same angular momentum quantum number ℓ.

v is $g(v) = v + 1$. This is plugged into eq. A.7 to calculate the normal mode partition function:

$$Q_i = \sum_{v=0}^{\infty} (v+1) {z_i}^v = \frac{1}{(1-z_i)^2}, \quad i \in \delta_d \tag{A.12}$$

The table shows that there is exactly one σ_g^+ state for every even v, so that the normal mode symmetry partition function becomes:

$$Q_{i,\sigma_g^+} = \sum_{k=0}^{\infty} {z_i}^{2k} = \frac{1-z_i}{1+z_i} Q_i, \quad i \in \delta_d \tag{A.13}$$

Similarly to eq A.11 the partition function for π symmetry counts all molecules in the degenerate normal mode that are not counted by Q_{i,σ_g^+}:

$$Q_{i,\pi} = Q_i - Q_{i,\sigma_g^+} = \frac{2z_i}{1+z_i} Q_i, \quad i \in \delta_d \tag{A.14}$$

We take a small sidestep here to assess whether ignoring the absence of rotational levels with $J < |\ell|$ leads to significant errors. The partition function that counts all levels with a given ℓ within the bending normal mode is given by:

$$Q_\ell = \sum_{k=0}^{\infty} {z_i}^{|\ell|+2k} = {z_i}^{|\ell|}\frac{1-z_i}{1+z_i}Q_i, \quad i \in \delta_d \tag{A.15}$$

Accounting for the absence of rotational levels with $J < |\ell|$ is the same as summing the ℓ quantum *up to* a maximum of J. The bending normal mode partition function can thus be calculated using:

$$Q_{i,\pi}(J) = 2\sum_{\ell=1}^{J} Q_\ell = \frac{2z_i(1-{z_i}^J)}{1+z_i}Q_i, \quad i \in \delta_d \tag{A.16}$$

The factor 2 accounts for negative ℓ-values. By comparing this to eq. A.14 we find that the difference is given by the term ${z_i}^J$, which will go rapidly to zero for increasing J. In conclusion, ignoring the absence of rotational levels with $J < |\ell|$ does not lead to a significant error.

Appendix A.4. Apparent degeneracy

It is now possible to calculate ΔQ_{Σ^+}, which was the remaining unknown for finding the apparent degeneracy, by using the expressions for the vibrational symmetry partition functions. The molecular partition function is calculated by taking the product over the partition functions of the normal modes:

$$Q_{vib} = \prod_i Q_i \tag{A.17}$$

In table A2 we see that the molecule can only be in Σ_g^+ or Σ_u^+ if every degenerate normal mode is in a σ_g^+ symmetry, since any π normal mode will make the molecular symmetry also Π. For the symmetric stretch this condition is trivially met because it always has a σ_g^+ symmetry. Consequently, determining which of Σ_g^+ or Σ_u^+ is the symmetry of the molecule, ultimately depends on the symmetry of the asymmetric stretch modes. It would be tempting to demand the asymmetric stretch normal modes also to be σ_g^+ in order to get a Σ_g^+ molecule, but there is a small nuance to be made here. For longer molecules it is in principle possible to have an arbitrary number of asymmetric stretch normal modes. According to table A2, if an even number of these modes have σ_u^+ symmetry, the molecule will have Σ_g^+ symmetry. These combinations are taken into account by directly calculating the difference partition function ΔQ_{Σ^+} and taking the difference $Q_{i,\sigma_g^+} - Q_{i,\sigma_u^+}$ individually for each asymmetric stretch normal mode:

$$\Delta Q_{\Sigma^+} = \prod_{i\in\nu_s} Q_{i,\sigma_g^+} \cdot \prod_{i\in\nu_{as}} \left(Q_{i,\sigma_g^+} - Q_{i,\sigma_u^+}\right) \cdot \prod_{i\in\delta_d} Q_{i,\sigma_g^+} \tag{A.18}$$

Combining this with eqs A.9 to A.13 yields:

$$\Delta Q_{\Sigma^+} = \prod_{i\in\nu_s} Q_i \cdot \prod_{i\in\nu_{as}} \frac{1-z_i}{1+z_i}Q_i \cdot \prod_{i\in\delta_d} \frac{1-z_i}{1+z_i}Q_i \tag{A.19}$$

Surprisingly, the products for the bending and asymmetric stretch normal modes have the same form and can therefore be grouped together. Combining eq A.19 with eq A.17 we can rewrite eq A.6 to:

$$\tilde{g}_{e/o} = \frac{1}{2}(g_s + g_a) \pm \frac{1}{2}(g_s - g_a) \prod_{i \in \delta_d, \nu_{as}} \frac{1 - z_i}{1 + z_i} \tag{A.20}$$

Here the plus is for even and the minus for odd rotational levels, and the product is taken over only the bending (δ_d) and asymmetric stretch (ν_{as}) normal modes. We can now readily evaluate this expression by plugging in the degeneracies g_s and g_a for CO_2 and C_2H_2, to arrive at the explicit expressions for the apparent nuclear degeneracy:

$$CO_2 : \tilde{g}_{e/o} = \frac{1}{2} \pm \frac{1}{2} \left(\frac{1 - z_2}{1 + z_2}\right) \left(\frac{1 - z_3}{1 + z_3}\right) \tag{A.21}$$

$$C_2H_2 : \tilde{g}_{e/o} = 2 \mp \left(\frac{1 - z_3}{1 + z_3}\right) \left(\frac{1 - z_4}{1 + z_4}\right) \left(\frac{1 - z_5}{1 + z_5}\right) \tag{A.22}$$

With:

$$z_i = \exp -\frac{hc\omega_i}{kT_i} \tag{A.23}$$

In conclusion, we have derived the relationship between the apparent nucelar degeneracy and the vibrational temperature. This relationship emerged because of the alternation of nuclear degeneracies in higher vibrational levels of the bending and asymmetric stretch normal modes.